Journal of Magnetic Resonance **140,** 491–494 (1999)
Article ID jmre.1999.1870, available online at http://www.idealibrary.com on IDEAL®

The 2D {^{31}P} Spin-Echo-Difference Constant-Time [^{13}C, ^{1}H]-HMQC Experiment for Simultaneous Determination of $^{3}J_{H3'P}$ and $^{3}J_{C4'P}$ in ^{13}C-Labeled Nucleic Acids and Their Protein Complexes

Thomas Szyperski,*[,1] César Fernández,* Akira Ono,† Kurt Wüthrich,* and Masatsune Kainosho†

*Institut für Molekularbiologie und Biophysik, Eidgenössische Technische Hochschule-Hönggerberg, CH-8093 Zürich, Switzerland; and †Department of Chemistry, Faculty of Science, Tokyo Metropolitan University, 1-1 Minamiohsawa, Hachioji 192-03, Japan

Received April 21, 1999; revised July 6, 1999

A two-dimensional {^{31}P} spin-echo-difference constant-time [^{13}C, ^{1}H]-HMQC experiment (2D {^{31}P}-sedct-[^{13}C, ^{1}H]-HMQC) is introduced for measurements of $^{3}J_{C4'P}$ and $^{3}J_{H3'P}$ scalar couplings in large ^{13}C-labeled nucleic acids and in DNA–protein complexes. This experiment makes use of the fact that ^{1}H–^{13}C multiple-quantum coherences in macromolecules relax more slowly than the corresponding ^{13}C single-quantum coherences. $^{3}J_{C4'P}$ and $^{3}J_{H3'P}$ are related via Karplus-type functions with the phosphodiester torsion angles β and ϵ, respectively, and their experimental assessment therefore contributes to further improved quality of NMR solution structures. Data are presented for a uniformly ^{13}C, ^{15}N-labeled 14-base-pair DNA duplex, both free in solution and in a 17-kDa protein–DNA complex. © 1999 Academic Press

Key Words: **$^{3}J_{C4'P}$ and $^{3}J_{H3'P}$ scalar couplings; protein–nucleic acid complexes; multiple-quantum coherence; NMR structure determination; ^{13}C labeling.**

Nuclear magnetic resonance (NMR) structure determination of nucleic acids makes extensive use of vicinal scalar couplings (*1–3*). In particular, $^{3}J_{C4'P}$ and $^{3}J_{H3'P}$ are related with the torsion angles β and ϵ, respectively (*4*), which define the phosphodiester backbone conformation. In this Communication we present the 2D {^{31}P}-sedct-[^{13}C, ^{1}H]-HMQC experiment, a spin-echo-difference constant-time (ct) scheme (*5–9*), for measurement of $^{3}J_{C4'P}$ and $^{3}J_{H3'P}$ in ^{13}C-labeled nucleic acids (*10–17*) and their protein complexes. The couplings were determined for a uniformly ^{13}C/^{15}N-labeled 14-base-pair DNA duplex prepared by solid-phase synthesis, both free in solution and in the 17-kDa *Antp*(*C39S*) homeodomain–DNA complex (*15*).

The 2D {^{31}P}-sedct-[^{13}C, ^{1}H]-HSQC (*6, 8*) and 2D {^{31}P}-sed dual ct-[^{13}C, ^{1}H]-HSQC (*7*) experiments measure signal attenuation of cross peaks that are caused by passive $^{3}J_{CP}$ and $^{3}J_{HP}$ couplings, respectively. Use for larger systems is limited by rapid T_2 relaxation of ^{1}H and ^{13}C single-quantum coherences (SQC). The new 2D {^{31}P}-sedct-[^{13}C, ^{1}H]-HMQC scheme (Fig. 1a) takes advantage of the fact that ^{1}H–^{13}C multiple-quantum coherence (MQC) relaxes more slowly than ^{13}C single-quantum coherence (*19–22*). Furthermore, when compared with HSQC, 2D [^{13}C, ^{1}H]-HMQC (*22*) exhibits greatly enhanced sensitivity for CH groups in larger macromolecules. With 2D {^{31}P}-sedct-[^{13}C, ^{1}H]-HMQC, only a single reference experiment needs to be recorded for measurement of both $^{3}J_{C4'P}$ and $^{3}J_{H3'P}$, and no additional ct delay is required for attenuation by $^{3}J_{H3'P}$, since the delays for the dephasing of ^{1}H–^{13}C MQC by $^{3}J_{C4'P}$ and $^{3}J_{H3'P}$ are overlaid (Fig. 1a). Overall, only three subspectra are thus recorded in measurements of the two types of couplings: (I) a reference subspectrum with decoupling of both $^{3}J_{HP}$ and $^{3}J_{CP}$ during the ct delay, (II) a subspectrum with decoupling of $^{3}J_{CP}$, and (III) a subspectrum with decoupling of $^{3}J_{HP}$. Signal attenuation in (II) and (III) relative to (I) yields $^{3}J_{H3'P}$ and $^{3}J_{C4'P}$, respectively (*6–8*). A potential drawback of 2D {^{31}P}-sedct-[^{13}C, ^{1}H]-HMQC arises from the fact that measurements of $^{3}J_{C2'P}$ and $^{3}J_{H5'P}$ are prevented by $^{2}J_{HH}$ dephasing during the ct delay. However, the HSQC measurements cannot in general provide complete sets of these data either. Due to severe spectral overlap of the C5′H signals (*23*) in 2D {^{31}P}-sed dual ct-[^{13}C, ^{1}H]-HSQC, only three $^{3}J_{H5'P}$ or $^{3}J_{H5''P}$ couplings could be obtained for the *Antp*(*C39S*)–DNA complex, and five such couplings were measured for the free DNA.

In view of the limited chemical shift dispersion of the H3′, H4′, and H5′/H5″ resonances (*1, 23*), we did not use a ^{1}H spin lock for suppression of ^{1}H–^{1}H J dephasing during the ct delay, τ_{ct} (*20*), since even a weak continuous-wave spin lock would cause significant Hartmann–Hahn transfer of ^{1}H magnetization (*22*) and thus prevent accurate data analysis. For H3′, the sugar pucker (*4*) determines $^{3}J_{HH}$ dephasing by $^{3}J_{H3'H4'}$, $^{3}J_{H3'H2'}$, and $^{3}J_{H3'H2''}$. Losses are minimal and maximal in C2′-endo and C3′-endo, respectively (*1–3*). For $\tau_{ct} = 1/^{1}J_{CC} = 23$ ms and $\tau_{ct} = 2/^{1}J_{CC} = 46$ ms, the losses in an ideal B-DNA (A-RNA) helix are 7% (27%) and 27% (79%), respectively (the pucker

[1] To whom correspondence should be addressed at Department of Chemistry, State University of New York at Buffalo, 816 Natural Sciences Complex, Buffalo, NY 14260.

1090-7807/99 $30.00

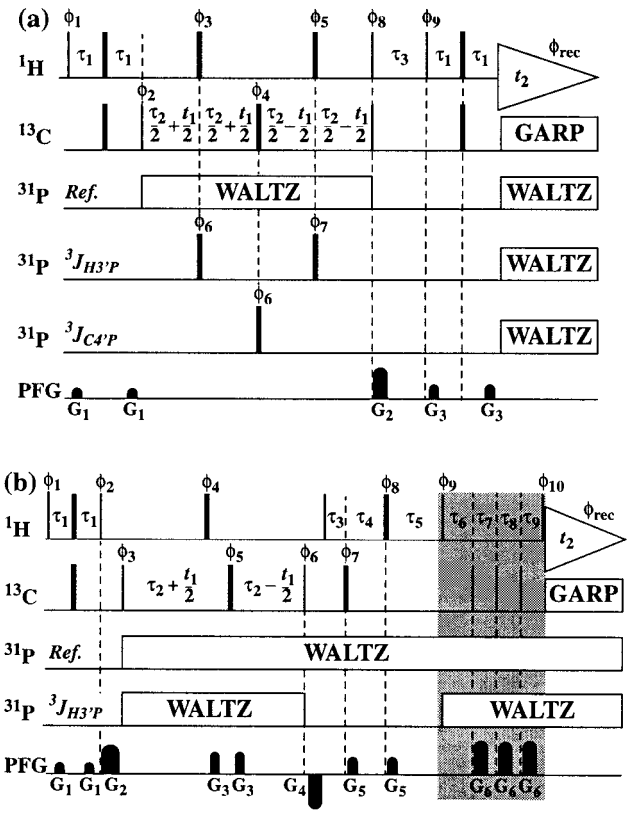

FIG. 1. (a) Pulse scheme of 2D {^{31}P}-sedct-[^{13}C, ^{1}H]-HMQC. The ^{31}P RF pulse sequences denoted as "Ref.," "$^3J_{H3'P}$," and "$^3J_{C4'P}$" were applied to record the reference spectrum, and for the measurements of $^3J_{H3'P}$ and $^3J_{C4'P}$, respectively. Suppression of residual HDO magnetization is achieved with the z filter [90°(ϕ_8)–τ_3–90°(ϕ_9)]. Delays: τ_1 = 1.5 ms, τ_2 = 11.5 ms (yielding τ_{ct} = 23 ms) or 23 ms (yielding τ_{ct} = 46 ms), and τ_3 = 2 ms. Durations and amplitudes of the sine-bell-shaped pulsed field gradients (PFG): 400 μs and 5 G/cm for G_1, 1 ms and 50 G/cm for G_2, and 400 μs and 10 G/cm for G_3. Phase cycling: $\phi_1 = x$; $\phi_2 = x, -x$; $\phi_3 = 8\{x\}, 8\{-x\}$; $\phi_4 = 2\{x\}, 2\{-x\}, 2\{y\}, 2\{-y\}$; $\phi_5 = 16\{x\}, 16\{-x\}$; $\phi_6 = x, -x$; $\phi_7 = 2\{x\}, 2\{-x\}$; $\phi_8 = y$; $\phi_9 = -y$; $\phi_{rec} = x, 2\{-x\}, x$. (b) Pulse scheme of 2D {^{31}P}-sed dual ct-[^{13}C, ^{1}H]-HSQC (*7*) for the measurement of $^3J_{HP}$ scalar couplings extended by a cluster of radiofrequency and PFG pulses (indicated in the gray box) to dephase ^{1}H–^{1}H antiphase magnetization that might emerge during the evolution of $^3J_{HP}$ (see below). Delays: τ_1 = 1.5 ms, τ_2 = 11.5 ms (for τ_{ct} = 23 ms) or 23 ms (for τ_{ct} = 46 ms), τ_3 = 1.72 ms, τ_4 = 6.79 ms, τ_5 = 8.51 ms, τ_6 = 3.57 ms, τ_7 = 3 ms, τ_8 = 2.83 ms, and τ_9 = 2.5 ms. The evolution period for dephasing by ^{31}P is given by $\tau_P = \tau_3 + \tau_4 + \tau_5 + 180°(^{13}C) + 180°(^1H)$ = 17.0588 ms. Durations and amplitudes of the sine-bell-shaped PFGs: 400 μs and 5 G/cm for G_1, 3 ms and 40 G/cm for G_2, 300 μs and 30 G/cm for G_3, 1 ms and −50 G/cm for G_4, 400 μs and 15 G/cm for G_5, and 2 ms and 50 G/cm for G_6. Phase cycling: $\phi_1 = x$; $\phi_2 = y, -y$; $\phi_3 = x$; $\phi_4 = 2\{x\}, 2\{-x\}$; $\phi_5 = 2\{x\}, 2\{y\}, 2\{-x\}, 2\{-y\}$; $\phi_6 = 8\{x\}, 8\{-x\}$; $\phi_7 = x, -x$; $\phi_8 = 2\{x\}, 2\{-x\}$; $\phi_9 = y$; $\phi_{10} = 8\{-y\}, 8\{y\}$; $\phi_{rec} = x, 2\{-x\}, x$. Dephasing of ^{1}H–^{1}H antiphase magnetization emerging during τ_P: the 90°(^{1}H) pulse denoted with ϕ_9 stores the desired ^{1}H in-phase magnetization along z. All terms that have to be dephased then possess transverse proton product operators. During [τ_x–90°(^{13}C)–G_6] (with x = 7, 8, 9) these terms evolve into antiphase with respect to ^{13}C, are converted into ^{1}H–^{13}C multiple-spin coherence, and are dephased. The aforementioned variable durations of τ_7, τ_8, and τ_9 ensure effective dephasing for $^1J_{HC}$ values in the range 140–180 Hz. The last 90°(^{1}H) pulse recreates ^{1}H SQC for detection. For (a) and (b), rectangular 90° and 180° pulses are indicated by thin and thick black vertical bars, respectively, and phases are indicated above the pulses. RF pulse lengths: 180°(^{1}H) = 11.8 μs, 180°(^{13}C) = 27 μs, and 180°(^{31}P) = 106 μs. Where no radiofrequency phase is marked, the pulse is applied along x. For the ^{1}H pulses the carrier was placed at the position of the water line at 4.64 ppm, and the ^{13}C and ^{31}P carriers were set to 65 and −2.1 ppm, respectively. A GARP sequence (*27*) with RF = 3.3 kHz was used to decouple ^{13}C during proton detection, and a WALTZ16 sequence (*28*) with RF = 0.6 kHz to decouple ^{31}P during carbon chemical shift evolution. Quadrature detection in t_1(^{13}C) is accomplished by alternating the phases ϕ_2 or ϕ_3 in (a) and (b), respectively, according to States–TPPI (*29*).

amplitudes were assumed to be 35°). For H4′, the sugar pucker and the backbone dihedral angle γ (*4*) determine $^3J_{H3'H4'}$, $^3J_{H4'H5'}$, and $^3J_{H4'H5''}$. The losses are, for τ_{ct} = 23 ms and τ_{ct} = 46 ms, respectively, 2 and 9% for C2′-endo/γ^+, 14 and 50% for C3′-endo/γ^+, 28 and 89% for C2′-endo/γ^t, 36 and 94% for C3′-endo/γ^t, 30 and 91% for C2′-endo/γ^-, and 38 and 95% for C3′-endo/γ^-. Hence, measurements performed with τ_{ct} = 23 ms are not critically affected by losses from $^3J_{HH}$ dephasing. Moreover, τ_{ct} = 46 ms yields less than 50% signal reduction for both measurement of $^3J_{H3'P}$ in nucleotides with a C2′-endo sugar pucker, which applies to most DNA duplexes, and measurement of $^3J_{C4'P}$ in nucleotides with γ^+, which is usually observed in both DNA and RNA (*24*). In fact, a dramatic decrease in intensity relative to the C4′H signals of nucleotides with γ^+, which might be registered between two experiments with τ_{ct} = 23 ms and τ_{ct} = 46 ms, would yield the structural information that the corresponding torsion angle is either γ^t or γ^-. The new scheme can thus be expected to be the experiment of choice for larger systems, because losses due to $^3J_{HH}$ dephasing are either overcompensated by the gain arising from slower relaxation of HMQC (*22*) or provide constraints for γ.

To compare 2D {^{31}P}-sedct-[^{13}C, ^{1}H]-HMQC with the corresponding HSQC experiments, we modified the original 2D {^{31}P}-sed dual ct-[^{13}C, ^{1}H]-HSQC scheme, which had been designed for selectively deuterated nucleic acids (*7*), to ensure that ^{1}H–^{1}H antiphase magnetization that emerges during the evolution of $^3J_{HP}$ is dephased prior to detection (see the legend to Fig. 1b). Figure 2 affords a comparison of corresponding HMQC and HSQC reference subspectra. For the 17-kDa *Antp*(*C39S*)–DNA complex we obtained average sensitivity gains of 1.5 to 2.4. This is in agreement with predictions (*22*) and significantly larger gains can be expected for larger systems (e.g., nucleic acids with more than 50 nucleotides), which places 2D {^{31}P}-sedct-[^{13}C, ^{1}H]-HMQC in a unique position for studies of $^3J_{H3'P}$ and $^3J_{C4'P}$ in large nucleic acids and nucleic acid–protein complexes. Overlap in the spectral regions of the C3′–H3′ and C4′–H4′ cross peaks (Fig. 2) will foreseeably become a limiting factor for systems with more than about 30 nucleotides, in particular at τ_{ct} = 23 ms, so that preparation of segmentally or selectively ^{13}C-labeled nucleic acids (*10–17*) will be

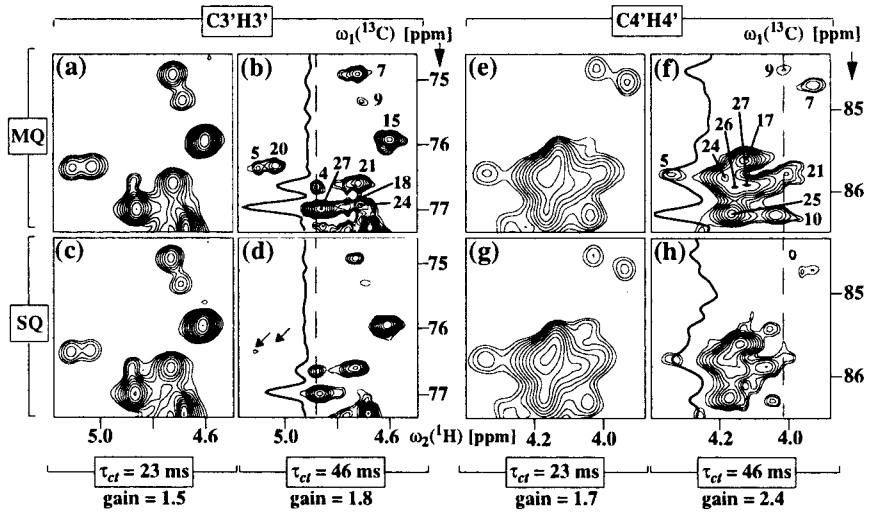

FIG. 2. Spectral regions comprising C3′H3′ (a–d) and C4′H4′ (e–h) cross peaks taken from the ^{31}P-decoupled reference subspectra of 2D {^{31}P}-sed-[^{13}C, ^{1}H]-HMQC/HSQC experiments recorded for measurement of $^{3}J_{H3'P}$ and $^{3}J_{C4'P}$ couplings in the *Antennapedia* homeodomain–DNA complex (concentration 1.5 mM, T = 36°C, pH 6.0, solvent D_2O). Panels a, b, e, and f were taken from a 2D {^{31}P}-sedct-[^{13}C, ^{1}H]-HMQC spectrum recorded with the pulse scheme of Fig. 1a. Panels c and d were taken from 2D {^{31}P}-sed-dual ct-[^{13}C, ^{1}H]-HSQC (Fig. 1b), and g and h from 2D {^{31}P}-sedct-[^{13}C, ^{1}H]-HSQC spectra. The τ_{ct} values used are indicated below the corresponding panels. (Note the increased resolution along ω_1(^{13}C) for longer τ_{ct}.) The average gain in signal-to-noise when comparing HMQC and HSQC is given below each vertical pair of panels. In b, d, f, and h, a cross section taken along the dashed lines is shown. The arrows in d indicate two peaks which are absent in the HSQC spectrum, but are clearly observed by HMQC in b. All spectra were recorded on a Bruker DRX-500 spectrometer equipped with a ^{1}H-{^{13}C, ^{31}P} triple-resonance probe. For the experiments with τ_{ct} = 23 ms, 376(t_1) × 512(t_2) complex points were accumulated, with $t_{1,max}$(^{13}C) = 22.5 ms and $t_{2,max}$(^{1}H) = 85.2 ms, yielding a measurement time of about 7 h per subspectrum. For τ_{ct} = 46 ms, 754(t_1) × 512(t_2) complex points were accumulated, with $t_{1,max}$ (^{13}C) = 45.0 ms and $t_{2,max}$(^{1}H) = 85.2 ms, yielding a measurement time of about 21 h per spectrum. Fully and partially ^{13}C, ^{15}N-labeled DNA oligomers were synthesized on a DNA synthesizer (Applied Biosystems Model 392–28) by the solid-phase phosphoramidite method, using isotopically labeled monomer units that had been synthesized according to the previously described general strategy (*30*). Approximately 1 μmol of oligomer was obtained from 5 μmol of nucleoside bound to the resin, and the purity of labeled oligomers was higher than 99% as estimated by HPLC analysis on a C-18 column (Inertsil ODS-2, GL Science). A full account of the synthesis will be presented elsewhere.

required to make full use of the potential of 2D {^{31}P}-sedct-[^{13}C, ^{1}H]-HMQC for studies of large nucleic acids.

^{13}C4′ is coupled to 5′- and 3′-standing ^{31}P spins via $^{3}J_{C4'P5'}$ and $^{3}J_{C4'P3'}$. Hence, the C4′–H4′ cross peaks in 2D {^{31}P}-sedct-[^{13}C, ^{1}H]-HMQC are attenuated by two scalar couplings, and two experiments acquired with different τ_{ct} are necessary to extract the two values (*25*) (Fig. 3). Moreover, it remains to unambiguously assign $^{3}J_{C4'P5'}$ and $^{3}J_{C4'P3}$. This can be achieved if measurement of $^{3}J_{H3'P}$ and/or $^{3}J_{C2'P}$ allows a sufficiently precise prediction of $^{3}J_{C4'P3'}$ via corresponding Karplus-type functions (*1–3*) for the torsion angle ϵ, so that the second coupling can be assigned to $^{3}J_{C4'P5}$ and translated into a constraint for β. For smaller ^{13}C-labeled nucleic acids, the assignment may also be supported by inspection of peak intensities registered in 3D HCP (*22*). Alternatively, the two values might be used as a pair of constraints to be assigned individually during structure refinement. Since $^{3}J_{H3'P}$ from 2D {^{31}P}-sedct-[^{13}C, ^{1}H]-HMQC and $^{3}J_{C2'P}$ from 2D {^{31}P}-sedct-[^{13}C, ^{1}H]-HSQC were available in the present study (*8*), these were primarily used for assigning $^{3}J_{C4'P}$. Overall, for the *Antp*(*C39S*)–DNA complex we obtained at τ_{ct} = 23 ms and τ_{ct} = 46 ms, respectively, 10 and 17 out of 28 $^{3}J_{H3'P}$ values, and 11 and 18 out of 26 $^{3}J_{C4'P5'}$ and $^{3}J_{C4'P3'}$ couplings. For the free DNA, the corresponding values at τ_{ct} = 23 ms and τ_{ct} = 46 ms, respectively, are 12 and 21 for $^{3}J_{H3'P}$, and 10 and 14 for the $^{3}J_{C4'P5'}$ and $^{3}J_{C4'P3'}$ values. We also performed 2D {^{31}P}-sedct-[^{13}C, ^{1}H]-HMQC for the same DNA duplex free in solution, which was partially ^{13}C/^{15}N-labeled only at those nucleotides which contact the protein in the *Antp*(*C39S*)–DNA complex (*8, 18*). We obtained at τ_{ct} = 23 ms and τ_{ct} = 46 ms, respectively, 7 and 2 additional $^{3}J_{H3'P}$ values, and 2 and 3 additional $^{3}J_{C4'P5'}$ and $^{3}J_{C4'P3'}$ couplings. Overall, 24 and 22 constraints could be derived from heteronuclear scalar couplings for the angle ϵ for the free and complexed DNA, respectively, and 12 and 11 constraints were correspondingly obtained for the backbone dihedral angle β to determine high-quality NMR solution structures of the DNA duplex and the protein–DNA complex (*26*).

In conclusion, the use of 2D {^{31}P}-sedct-[^{13}C, ^{1}H]-HMQC with uniformly ^{13}C-labeled DNA enabled the determination of $^{3}J_{C4'P}$ and $^{3}J_{H3'P}$ couplings in a DNA–protein complex of size 17 kDa. The 2D ct-[^{13}C, ^{1}H]-HMQC experiment can be expected to offer a unique potential of providing conformational constraints for the torsion angles β and ϵ in nucleic acids and nucleic acid–protein complexes with molecular weights well above 20 kDa.

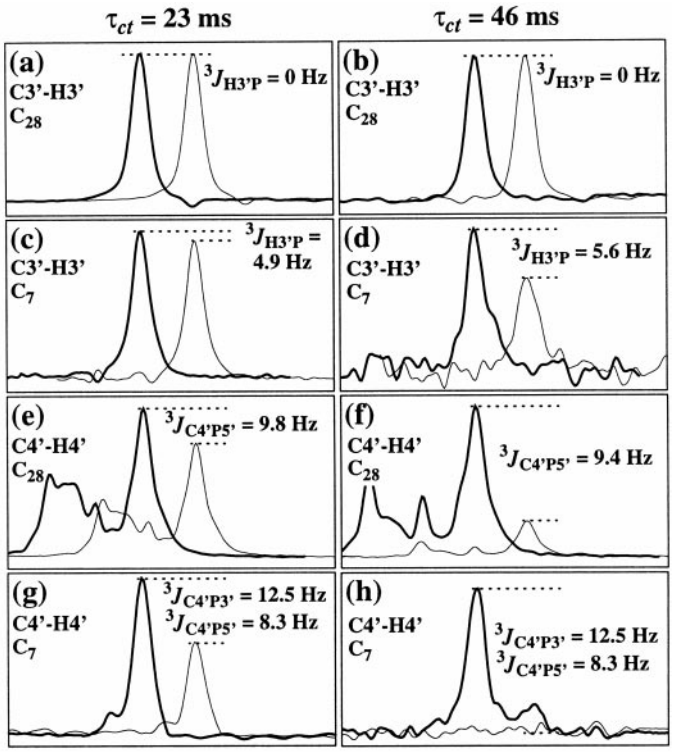

FIG. 3. Cross sections along $\omega_2(^1H)$ through the C3′–H3′ and C4′–H4′ cross peaks of C_7 and C_{28} from corresponding 2D {^{31}P}-sedct-[^{13}C,^{1}H]-HMQC subspectra recorded with (thick lines) and without (thin lines) ^{31}P decoupling. As indicated above the figure, the cross sections on the left were recorded with $\tau_{ct} = 23$ ms, and those on the right with $\tau_{ct} = 46$ ms (see the legend to Fig. 2). The dotted lines indicate the peak heights with and without ^{31}P decoupling; the difference between these peak heights is the quantity of interest. (a, b) Cross sections containing the C3′–H3′ cross peak of C_{28}, which has no ^{31}P coupling because the DNA studied has no 3′-terminal phosphate group. (c, d) Cross sections containing the C3′–H3′ cross peak of C_7. (e, f) Cross sections containing the C4′–H4′ cross peak of the 3′-terminal C_{28}. (g, h) Cross sections containing the C4′–H4′ cross peak of C_7, which is subject to two ^{31}P couplings. The values of the spin–spin coupling constants calculated from these data are indicated in each panel.

ACKNOWLEDGMENTS

We thank Dr. H. Iwai for the preparation of the *Antennapedia* homeodomain used in this study. Financial support was obtained from the Schweizerischer Nationalfonds (Project 31–32033.96), from the ETH Zürich for a special grant within the framework of the Swiss/Japanese R & D Roundtable Collaboration, and by CREST (Core Research for Evolutional Science and Technology) of the Japan Science and Technology Corporation (JST).

REFERENCES

1. K. Wüthrich, "NMR of Proteins and Nucleic Acids," Wiley, New York (1986).
2. S. S. Wijmenga, M. M. W. Mooren, and C. W. Hilbers, *in* "NMR of Macromolecules" (G. C. K. Roberts, Ed.), pp. 217–288, Oxford Univ. Press, Oxford (1993).
3. T. Szyperski, C. Fernández, A. Ono, M. Kainosho, and K. Wüthrich, *J. Am. Chem Soc.* **120,** 821–822 (1998).
4. W. Saenger, "Principles of Nucleic Acid Structure," Springer-Verlag, Berlin/New York (1984).
5. G. W. Vuister, A. C. Wang, and A. Bax, *J. Am. Chem Soc.* **115,** 5334–5335 (1993).
6. P. Legault, F. M. Jucker, and A. Pardi, *FEBS Lett.* **362,** 156–160 (1995).
7. S. Tate, Y. Kubo, A. Ono, and M. Kainosho, *J. Am. Chem Soc.* **117,** 7277–7278 (1995).
8. T. Szyperski, A. Ono, C. Fernández, H. Iwai, S. Tate, K. Wüthrich, and M. Kainosho, *J. Am. Chem. Soc.* **119,** 7277–7278 (1997).
9. G. M. Clore, E. C. Murphy, A. M. Gronenborn, and A. Bax, *J. Magn. Reson.* **134,** 164–167 (1998).
10. E. P. Nikonowicz, A. Sirr, P. Legault, F. M. Jucker, L. M. Baer, and A. Pardi, *Nucleic Acids Res.* **20,** 4507–4513 (1992).
11. A. Ono, S. Tate, Y. A. Ishido, and M. Kainosho, *J. Biomol. NMR* **4,** 581–586 (1994).
12. S. Quant, R. W. Wechselberger, M. A. Wolter, K. H. Worner, P. Schell, J. W. Engels, C. Griesinger, and H. Schwalbe, *Tetrahedron Lett.* **35,** 6649–6652 (1994).
13. C. Richter, B. Reif, K. Worner, S. Quant, J. P. Marino, J. W. Engels, and H. Schwalbe, *J. Biomol. NMR* **12,** 223–230 (1998).
14. D. P. Zimmer and D. M. Crothers, *Proc. Natl. Acad. Sci. USA* **92,** 3091–3095 (1995).
15. D. E. Smith, J.-Y. Su, and F. M. Jucker, *J. Biomol. NMR* **10,** 245–253 (1997).
16. G. Mer and W. J. Chazin, *J. Am. Chem. Soc.* **120,** 607–608 (1998).
17. J. E. Masse, P. Bortmann, T. Dieckmann, and J. Feigon, *J. Nucleic Acids Res.* **26,** 2618–2624 (1998).
18. M. Billeter, Y. Q. Qian, G. Otting, M. Müller, W. Gehring, and K. Wüthrich, *J. Mol. Biol.* **234,** 1084–1097 (1993).
19. R. H. Griffey and A. G. Redfield, *Q. Rev. Biophys.* **19,** 51–82 (1987).
20. S. Grzesiek and A. Bax, *J. Biomol. NMR* **6,** 335–339 (1995).
21. O. Zerbe, T. Szyperski, M. Ottiger, and K. Wüthrich, *J. Biomol. NMR* **7,** 99–106 (1996).
22. J. P. Marino, J. L. Diener, P. B. Moore, and C. Griesinger, *J. Am. Chem. Soc.* **119,** 7361–7366 (1997).
23. C. Fernández, T. Szyperski, A. Ono, H. Iwai, S. Tate, M. Kainosho, and K. Wüthrich, *J. Biomol. NMR* **12,** 25–37 (1998).
24. B. Schneider, S. Neidle, and H. M. Berman, *Biopolymers* **42,** 113–124 (1997).
25. C. Sich, O. Ohlenschläger, R. Ramachandran, M. Görlach, and L. R. Brown, *Biochemistry* **36,** 13989–14002 (1997).
26. C. Fernández, T. Szyperski, M. Billeter, A. Ono, H. Iwai, M. Kainosho, and K. Wüthrich, *J. Mol. Biol.,* in press.
27. A. J. Shaka, P. B. Barker, and R. Freeman, *J. Magn. Reson.* **64,** 547–552 (1985).
28. A. J. Shaka, C. J. Lee, and A. J. Pines, *J. Magn. Reson.* **52,** 335–338 (1983).
29. D. Marion, K. Ikura, R. Tschudin, and A. Bax, *J. Magn. Reson.* **85,** 393–399 (1989).
30. A. Ono, S. Tate, and M. Kainosho, "Stable Isotope Applications in Biomolecular Structure and Mechanisms" (J. Trewhella, T. A. Cross, and C. J. Unkefer, Eds.), pp. 127–144, Los Alamos Natl. Lab., Los Alamos, NM (1994).